Characterising Chaos in Pilot Wave System

Chun-Hei Lam
Department of Mathematics, *MIT*

Submitted in part fulfilment of the requirements for the course
18.353 Non-linear Dynamics I: Chaos.

1 Preliminaries

The paper is dedicated to the analysis of motion of a small droplet bouncing on an oscillating surface of fluid. When the surface oscillate with a sufficiently high frequency, the droplet will not coalesce to the surface of fluid but rather bounce and/or walk. This is usually referred to *(Hydrodynamic) Pilot Wave Phenomenon*. Following the development of [1, 2] the horizontal displacement of the particle $x_p(t)$, averaged over one vertical bouncing period, can be modelled by the following integro-differential equation.

$$m\ddot{x_p}(t) + D\dot{x_p}(t) = -F\frac{\partial}{\partial x}h(x_p(t), t) \tag{1}$$

with

$$h(x,t) = \frac{A}{T_F}\int_{-\infty}^{t} \cos(k(x - x_p(s)))e^{-(t-s)/T_M}ds \tag{2}$$

Different implications of the parameters are tabulated below:

Variable	Implication	MLT Dimension
m	Mass of droplet	M
D	Drag coefficient	MT^{-1}
F	Time-Averaged vibration force	MLT^{-2}
T_F	Period of vibration force	T
A	Amplitude of wave of surface	L
k	Wave Number of pilot wave on surface	L^{-1}
T_M	Decay timescale	T

Table 1: Parameters of Pilot Wave Equation

1.1 Reducing the Equation

Non-Dimensionalisation: We introduce the new parameters for our convenience:

$$x(t) = k^{-1}X(t), \quad x_p(t) = k^{-1}X_p(t), \quad t = T_0\tau, \quad h = \frac{AT_0}{T_F}\bar{h}, \quad T_0 = \sqrt{\frac{DT_F}{FAk^2}}$$

From this we have

$$\frac{dx_p}{dt} = \frac{1}{kT_0}\frac{dX_p}{d\tau}, \quad \frac{d^2x_p}{d\tau^2} = \frac{1}{kT_0^2}\frac{d^2X_p}{d\tau^2}, \quad \frac{d\tau}{dt} = T_0$$

Slightly trickier is the manipulation of $h(x,t)$:

$$h(X,\tau) = \frac{AT_0}{T_F}\int_{-\infty}^{\tau} \cos(X(s) - X_p(s))\, e^{(\tau - s/T_0)/T_F}\, d\,(s/T_0) \tag{3}$$

Substituting all these expression we have

$$\begin{aligned}
\frac{m}{kT_0^2}\frac{d^2X_p}{d\tau^2} + \frac{D}{kT_0}\frac{dX_p}{d\tau} &= -F\frac{kAT_0}{T_F}\partial_X\bar{h} \\
\frac{mT_F}{Ak^2FT_0^3}\frac{d^2X_p}{d\tau^2} + \frac{DT_F}{Ak^2FT_0^2}\frac{dX_p}{d\tau} &= -\partial_X\bar{h}(X_p(\tau),\tau) \\
\kappa_0\frac{d^2X_p}{d\tau^2} + \frac{dX_p}{d\tau} &= -\partial_X\bar{h}(X_p(\tau),\tau)
\end{aligned}$$

with $\kappa_0 = m/DT_0$ and $\mu = T_0/T_M$

$$\bar{h}(X,\tau) = \int_{-\infty}^{\tau} \cos(X - X_p(s))\, e^{-\mu(\tau - s)}\, ds$$

This yields

$$\frac{\partial}{\partial X}\bar{h}(X,\tau) = -\int_{-\infty}^{\tau} \sin(X - X_p(s))\, e^{-\mu(\tau - s)}\, ds$$

Plug $X = X_p(t)$ ('projecting onto particle trajectory') yields

$$\kappa_0\frac{d^2X_p}{d\tau^2} + \frac{dX_p}{d\tau} = \int_{-\infty}^{\tau} \sin(X_p(\tau) - X_p(s))\, e^{-\mu(\tau - s)}\, ds \tag{4}$$

Here κ_0 can be seen as the inertia of the particle, while μ can be seen as decay rate. If κ_0 and μ is large then it is likely that the particle with not walk ($\dot{x}_p \to 0$). We abuse notation and write (4) as

$$\kappa_0\ddot{x_p} + \dot{x_p} = \int_{-\infty}^{t} \sin(x_p(t) - x_p(s))\, e^{-\mu(t - s)}\, ds \tag{5}$$

Reduction to 3D dynamical system: We write $v = \dot{x}_p$ and define

$$a(t) = \int_{-\infty}^{t} \cos(x_p(t) - x_p(s))\, e^{-\mu(t-s)}\, ds \tag{6a}$$

$$b(t) = -\int_{-\infty}^{t} \sin(x_p(t) - x_p(s))\, e^{-\mu(t-s)}\, ds \tag{6b}$$

Then $h(t, x)$ can be simplified as followed:

$$\begin{aligned}
&a(t)\cos(x - x_p(t)) + b(t)\sin(x - x_p(t)) \\
&= \int_{-\infty}^{t} (\cos(x_p(t) - x_p(s))\cos(x - x_p(t)) - \sin(x_p(t) - x_p(s))\sin(x - x_p(t)))\ e^{-\mu(t-s)}\, ds \\
&= \int_{-\infty}^{t} \cos(x - x_p(s))\, e^{-\mu(t-s)}\, ds = h(x, t)
\end{aligned}$$

Equation (5) can therefore be rewritten as

$$\kappa_0 \dot{v} + v + b = 0$$

Differentiating (6a) (under integral signs) yields

$$\dot{a} = 1 - \int_{-\infty}^{t} e^{-\mu(t-s)}(\dot{x_p}(t)\sin(x_p(t) - x_p(s)) + \mu\cos(x_p(t) - x_p(s))) = 1 + vb - \mu a$$

Similarly by differentiating (6b) yields

$$\dot{b} = -va - \mu b$$

As we write $\boldsymbol{x} := (v, a, b)$, we may collect the above equations to obtain the system

$$\dot{\boldsymbol{x}} = \begin{pmatrix} \dot{v} \\ \dot{a} \\ \dot{b} \end{pmatrix} = \boldsymbol{f}(v, a, b) = \begin{pmatrix} -\kappa_0^{-1} v - \kappa_0^{-1} b \\ 1 - \mu a + vb \\ -va - \mu b \end{pmatrix} \tag{7}$$

This is the pilot wave system we will analyse in this paper.

1.2 Simple Properties of the Pilot Wave System

1.2.1 Comparison with Lorenz System

It worth noticing that Pilot Wave System is very similar to Lorenz System. Consider the following Lorenz system in (x, y, z):

$$\begin{pmatrix} \dot{x} \\ \dot{y} \\ \dot{z} \end{pmatrix} = \begin{pmatrix} \sigma y - \sigma x \\ rx - y - rz \\ xy - \beta z \end{pmatrix} \tag{8}$$

Making the correspondences $x \leftrightarrow v$, $y \leftrightarrow -b$, $z \leftrightarrow r-a$, $\sigma \leftrightarrow \kappa_0^{-1}$, $\beta \leftrightarrow \mu$ and restricting $r = \beta^{-1} = \mu^{-1}$, we have

$$\begin{pmatrix} \dot{v} \\ \dot{a} \\ \dot{b} \end{pmatrix} = \begin{pmatrix} -\kappa_0^{-1} v - \kappa_0^{-1} b \\ 1 - \mu a + vb \\ -va - b \end{pmatrix} \tag{9}$$

So the pilot wave system is almost a Lorenz system except with a different dissipation term of b. In fact one can immediately conclude properties of pilot wave system analogous to the Lorenz system.

- Pilot wave system has a natural symmetry $(v, a, b) \to (-v, a, -b)$.
- The a-axis is invariant. In fact if trajectories starting on a-axis will have $v = b \equiv 0$ for all t. The system simplifies to $\dot{a} = 1 - \mu a$ and therefore the trajectory approaches to the fixed point $(0, \mu^{-1}, 0)$.

We will look at the fixed point $(0, \mu^{-1}, 0)$ in greater detail.

1.2.2 Positive Invariant Set and Stability of $(0, \mu^{-1}, 0)$

Note that div $\boldsymbol{f} = -(\kappa_0^{-1} + 2\mu)$. This indicate that if $S(t)$ is a closed, sufficiently smooth surface enclosing region with volume $V(t)$ in phase space, then $S(t)$ and $V(t)$ evolves with respect to $\boldsymbol{f}$ by

$$\frac{dV}{dt} = \int_V (\text{div } f)\, dV = -(\kappa_0^{-1} + 2\mu)V \tag{10}$$

So the volume $V(t)$ will decay exponentially like $\exp(-(\kappa_0^{-1} + 2\mu))$. This justifies the existence of a zero-volume attractive set. In particular, it rules out the existence of unstable fixed points and unstable periodic orbits.[3, 4]

One can check that $(0, \mu^{-1}, 0)$ is a fixed point of (7). When $\mu > 1$, the following is a Lyapunov Function of pilot wave system with minimum at $(0, \mu^{-1}, 0)$.

$$E_1(v, a, b) = \frac{1}{2}\left(\kappa_0 v^2 + \mu(a - \mu^{-1})^2 + \mu b^2\right) \tag{11}$$

The orbital derivative of E_1 is

$$\begin{aligned} \frac{dE_1}{dt} &= \frac{\partial E_1}{\partial v}\frac{dv}{dt} + \frac{\partial E_1}{\partial a}\frac{da}{dt} + \frac{\partial E_1}{\partial b}\frac{db}{dt} \\ &= \kappa_0 v(-\kappa_0^{-1}(v + b)) + \mu(a - \mu^{-1})(1 - \mu a + vb) + \mu b(-(va + \mu b)) \\ &= -\left(v(v + b) + (1 - \mu a)(1 - \mu a + vb) + \mu b(va + \mu b)\right) \\ &= -\left(v^2 + bv + (1 - \mu a)^2 + vb - \mu abv + \mu abv + \mu^2 b^2)\right) \\ &= -\left(v^2 + 2bv + \mu^2 b^2 + (1 - \mu a)^2\right) \\ &= -\left((v + b)^2 + (\mu^2 - 1)b^2 + (1 - \mu a)^2\right) \end{aligned}$$

When $\mu \geq 1$, $\dot{E}_1 \leq 0$, equality holds only at $(0, \mu^{-1}, 0)$. This directly show that $(0, \mu^{-1}, 0)$ is the *(only)* global attractor of the system. This corresponds to the case when the period of vibrational force is too long (frequency too low) for the particle to move horizontally. In this paper we will focus on the case when $0 < \mu < 1$.

Remark. One might wish to conclude that, similar to Lorenz system, there is a ellipsoid $\mathcal{E}$ positive invariant in the sense that, once the trajectory enter $\mathcal{E}$ it will not thereafter leaves it. It is rather difficult to use functional E_1 to make such conclusion when $\mu < 1$. Instead we consider the modified functional

$$E_2(v,a,b) = \frac{1}{2}\left(\kappa_0 v^2 + \mu(a+\mu^{-1})^2 + \mu b^2\right) \tag{12}$$

with orbital derivative

$$\begin{aligned}\frac{dE_2}{dt} &= \frac{\partial E_2}{\partial v}\frac{dv}{dt} + \frac{\partial E_2}{\partial a}\frac{da}{dt} + \frac{\partial E_2}{\partial b}\frac{db}{dt}\\ &= \kappa_0 v(-\kappa_0^{-1}(v+b)) + \mu(a+\mu^{-1})(1-\mu a + vb) + \mu b(-(va+\mu b))\\ &= -v^2 - bv + (1-\mu^2 a^2) + vb + \mu abv - \mu abv - \mu^2 b^2)\\ &= -\left(v^2 + \mu^2 a^2 + \mu^2 b^2\right) + 1\end{aligned}$$

Therefore the region when $\dot{E}_2 \geq 0$ is the ellipse

$$R = \left\{(v,a,b) \,|\, v^2 + \mu^2 a^2 + \mu^2 b^2 \leq 1\right\}$$

which is compact in $\mathbb{R}^3$. By Extreme Value Theorem E_2 is bounded in R. Let M be the bound. For sufficient small and positive ϵ we consider the ellipsoid

$$\mathcal{E} = \{(v,a,b) \,|\, E_2(v,a,b) \leq M + \epsilon\}$$

Then R is clearly a strict subset of E, and along $\partial\mathcal{E}$ we have $\dot{E}_2 < 0$. Any trajectories starting outside $\mathcal{E}$ will eventually enter ellipsoid $\mathcal{E}$ in finite time, and all trajectories pass inwards through $\partial\mathcal{E}$. Therefore any trajectories will eventually stay inside $\mathcal{E}$. The size of $\mathcal{E}$ can be obtained by using the method of Lagrange multiplier. [3]

To end this subsection we show that $(0,\mu^{-1},0)$ destablises when μ decreases through unity. We linearise the system and consider the Jacobian of $\boldsymbol{f}(v,a,b)$:

$$D\boldsymbol{f}(v,a,b) = \begin{pmatrix} -\kappa_0^{-1} & 0 & -\kappa_0^{-1} \\ b & -\mu & v \\ -a & -v & -\mu \end{pmatrix} \tag{13}$$

$$D\boldsymbol{f}(0,\mu^{-1},0) = \begin{pmatrix} -\kappa_0^{-1} & 0 & -\kappa_0^{-1} \\ 0 & -\mu & 0 \\ -\mu^{-1} & 0 & -\mu \end{pmatrix} \tag{14}$$

The characteristic equation of the Jacobian is

$$\begin{aligned}P(\lambda) &= (-\kappa_0^{-1} - \lambda)(-\mu-\lambda)^2 - \kappa_0^{-1}(-(-\mu-\lambda)(-\mu^{-1}))\\ &= (\lambda+\mu)((\lambda+\mu)(\lambda+\kappa_0^{-1}) - \kappa_0^{-1}\mu^{-1})\\ &= (\lambda+\mu)(\lambda^2 + (\kappa_0^{-1}+\mu)\lambda + (\kappa_0\mu)^{-1}(\mu^2-1))\end{aligned}$$

Notice that when $0 < \mu < 1$ the characteristic equation has three root (two positive and one negative) (i.e. the Jacobian has two positive and one negative eigenvalues):

$$\begin{aligned}
&\lambda = -\mu < 0, \\
&\lambda = \frac{-(\kappa_0^{-1} + \mu) + \sqrt{(\kappa_0^{-1} + \mu)^2 - 4(\kappa_0\mu)^{-1}(\mu^2 - 1)}}{2} > 0, \\
&\lambda = \frac{-(\kappa_0^{-1} + \mu) - \sqrt{(\kappa_0^{-1} + \mu)^2 - 4(\kappa_0\mu)^{-1}(\mu^2 - 1)}}{2} < 0
\end{aligned}$$

Therefore the point $(0, \mu^{-1}, 0)$ is a saddle when $\mu < 1$.

1.3 The Outline of Paper

Section 2 discusses the stability of the fixed points arised when $\mu < 1$. One could see that a subcritical Hopf bifurcation would occur as μ is decreased. Section 3 reports the behaviour of chaotic attractors after a subcritical Hopf bifurcation has occured.

2 The New Fixed Points

Let us go back to equation (7) to check if there are extra fixed points when $\mu < 1$: we are in fact solving the system

$$\begin{cases} -\kappa_0^{-1}(v + b) = 0 \\ 1 - \mu a + vb = 0 \\ -va - \mu b = 0 \end{cases}$$

First equation simplifies to $v = -b$. Substituting into third equation yields $v(\mu - a) = 0$. This time we let $\mu = a$. Plug into the second equation yields $1 - \mu^2 = v^2$. Since $\mu < 1$, we have $v = \pm\sqrt{1 - \mu^2}$ and $b = \mp\sqrt{1 - \mu^2}$. Therefore for small μ two extra fixed points $(\pm\sqrt{1 - \mu^2}, \mu, \mp\sqrt{1 - \mu^2})$, which we consider as *steady propulsion state*. These fixed points correspond to the steady propulsion of water droplets at a velocity of $\pm\sqrt{1 - \mu^2}$.

We analyse the Jacobian at the fixed point:

$$D\boldsymbol{f}(\pm\sqrt{1-\mu^2}, \mu, \mp\sqrt{1-\mu^2}) = \begin{pmatrix} -\kappa_0^{-1} & 0 & -\kappa_0^{-1} \\ \mp\sqrt{1-\mu^2} & -\mu & \pm\sqrt{1-\mu^2} \\ -\mu & \mp\sqrt{1-\mu^2} & -\mu \end{pmatrix} \tag{15}$$

This has characteristic polynomial

$$\begin{aligned}
Q(\lambda) &= (-\kappa_0^{-1} - \lambda)((-\mu - \lambda)^2 + (1 - \mu^2)) - \kappa_0^{-1}((1 - \mu^2) - (-\mu)(-\mu - \lambda)) \\
&= -(\lambda + \kappa_0^{-1})(\lambda^2 + 2\lambda\mu + 1) - \kappa_0^{-1}(1 - 2\mu^2 - \lambda\mu) \\
&= -\lambda^3 - 2\lambda^2\mu - \lambda - \kappa_0^{-1}\lambda^2 - 2\lambda\kappa_0^{-1}\mu - \kappa_0^{-1} - \kappa_0^{-1} + 2\kappa_0^{-1}\mu^2 + \lambda\kappa_0^{-1}\mu \\
&= -(\lambda^3 + (2\mu + \kappa_0^{-1})\lambda^2 + (\mu\kappa_0^{-1} + 1)\lambda + 2\kappa_0^{-1}(1 - \mu^2)) \\
&= -\kappa_0^{-1}(\kappa_0\lambda^3 + (2\mu\kappa_0 + 1)\lambda^2 + (\mu + \kappa_0)\lambda + 2(1 - \mu^2))
\end{aligned}$$

We fix κ_0 and discuss the evolution of the eigenvalues of Jacobian as Γ increases from 0 to 1.

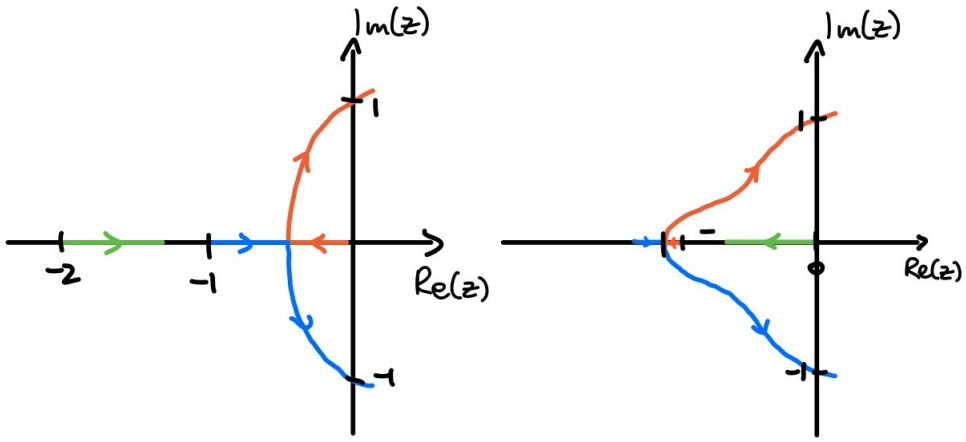

Figure 1: A sketch of trajectory as the eigenvalues evolve from $\Gamma = 0$ to $\Gamma = 1$. The left figure (a) corresponds to $\kappa_0 = 1$, while right figure (b) corresponds to $\kappa_0 = 3$

Initially (when $0 < \Gamma \ll 1$) all eigenvalues are real and negative. As Γ increases two of the real eigenvalues annihilate and a conjugate pair of eigenvalues are created. Γ will reach and pass a threshold (call it Γ_c and write $\mu_c = 1 - \Gamma_c$), at which the pair of fixed points now have eigenvalues with positive real part, hence turn to a pair of saddle nodes. [2] This is where a Hopf bifurcation occur. It is important to iterate the fact that when $\mu < \mu_c$ all eigenvalues have negative real parts and hence the pair of fixed points are stable. When $\mu = \mu_c$ the conjugate pair of eigenvalues is purely imaginary. We therefore assume at this particular value of μ, the eigenvalues are $\pm i\omega$ and ρ, with $\rho \in \mathbb{R}$ and $\omega > 0$. Applying Viete Formulae on the characteristic polynomial we have

$$\begin{cases} -(2\mu_c + \kappa_0^{-1}) = \rho \\ \mu_c \kappa_0^{-1} + 1 = \omega^2 \\ -2\kappa_0^{-1}(1 - \mu_c^2) = \rho\omega^2 \end{cases} \tag{16}$$

Plugging first two equations to the third yields

$$\begin{aligned} -(2\mu_c + \kappa_0^{-1})(\mu_c\kappa_0^{-1} + 1) &= -2\kappa_0^{-1}(1 - \mu_c^2) \\ \iff (2\mu_c\kappa_0 + 1)(\mu_c + \kappa_0) &= 2\kappa_0(1 - \mu_c^2) \\ \iff 4\kappa_0\mu_c^2 + (2\kappa_0^2 + 1)\mu_c - \kappa_0 &= 0 \\ \iff \mu_c &= \frac{1}{8\kappa_c}\left(-(2\kappa_0^2 + 1) + \sqrt{1 + 20\kappa_0^2 + 4\kappa_0^4}\right) \end{aligned}$$

It is important to note that $\mu_c \sim \kappa_0$ when $\kappa_0 \ll 1$ and $\mu_c \sim (2\kappa_0)^{-1}$ when $\kappa_0 \gg 1$. This indicates that μ_c does not blow up as κ_0 is small/large, and therefore Hopf bifurcation always occur.

The analysis above is not enough to conclude whether the Hopf bifurcation is *super-critical, subcritical or degenerate*. Computer simulations below suggests that the Hopf bifurcation is subcritical. One could justify rigorously by analysing a Landau equation from multi-scale arguments. [2]

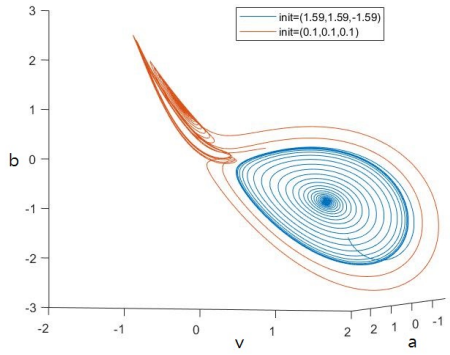

(a) $\mu = 0.3$ $(\Gamma = 0.7)$

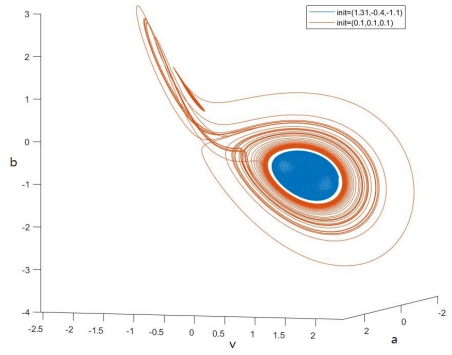

(b) $\mu = 0.26$ $(\Gamma = 0.74)$

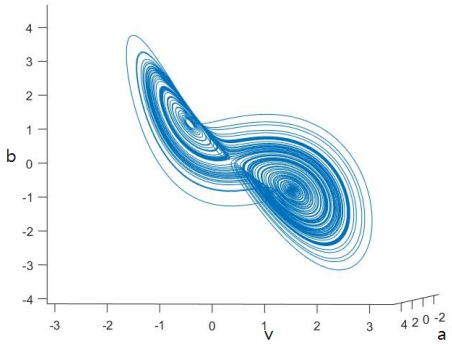

(c) $\mu = 0.2$ $(\Gamma = 0.8)$

Figure 2: Here we simulate different trajectories of pilot wave system at $\kappa_0 = 1$. In our case we have $\mu_c = 0.25$ $(\Gamma_c = 0.75)$. Figures (a) and (b): For each μ we have plotted two trajectories to illustrate the existence of unstable orbit around the pair of fixed points. Notice that the unstable orbit shrink as μ decreases to μ_c (Γ increases to μ_c). Figure (c): A trajectory starting at a point very closed to fixed point $(\sqrt{1-\mu^2}, \mu, -\sqrt{1-\mu^2})$ is plotted. Notice this fixed point is no longer stable.

3 The Route to Chaos

3.1 Existence of Homoclinic Bifurcations

Figure 2 has given us a hint that homoclinic bifurcation occurs as we increase μ from μ_c (decrease Γ from Γ_c). As we increase μ, the size of orbit will increase and eventually touches the rest-state fixed point $(0, \mu^{-1}, 0)$. At this particular $\mu = \mu_{e1}$ $(\Gamma = \Gamma_{e1})$ a homoclinic orbit starting/finishing at the rest-state fixed point is formed. When μ increases the homoclinic orbit explodes. [2]

Another way [3] to heuristically argue for existence of homoclinic orbit is to utilised the fact that the behaviour of trajectories starting at same initial point varies continuously with μ and κ_0. Depending on the size of μ, the trajectories converge to two different fixed points. This indicates that a homoclinic bifurcation has occured for some value of μ. The case when $\kappa_0 = 1$ is illustrated below.

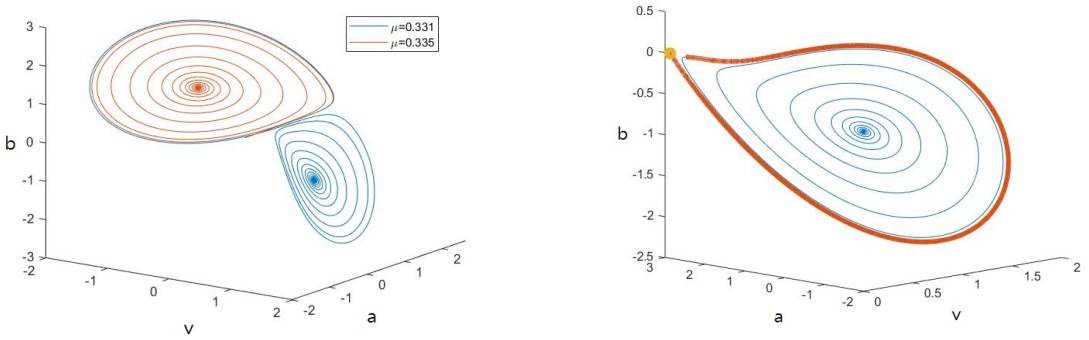

Figure 3: (a, left) Two trajectories starting at $(0.01, 0.01, 0.01)$ with $\mu = 0.331$ (blue) and $\mu = 0.335$ (red) are plotted. Notice a slight change of μ has a drastic change of the behaviour of trajectory (they converges to different fixed points.) (b, right) A numerical plot of the homoclinic orbit when $\mu \approx 0.3494$.

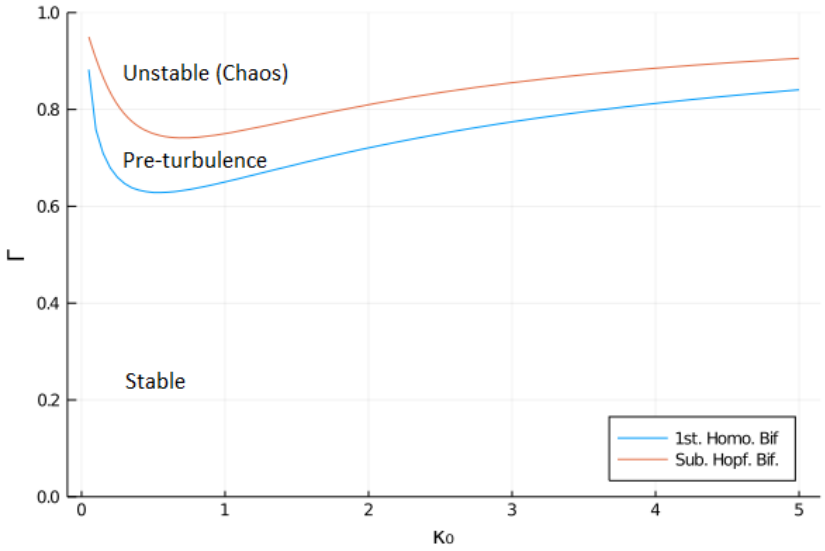

Figure 4: A numerical simulation has been done to estimate Γ_{e1}, the value of Γ when (first) homoclinic bifurcation occurs if we increase Γ from zero. The subcritical Hopf bifurcation curve has been superimposed.

3.2 Analysis of Lorenz Like Map

It is important to observe that when $\Gamma > \Gamma_{e1}$, the behaviour of trajectories turn chaotic. A trajectory with starting point very close to one of the stable propulsion state may end up converging to another stable propulsion state. This indicates that the stable manifolds of the stable propulsion states have been "twisted" as Γ exceed Γ_{e1}, which lead to more homoclinic bifurcations as Γ further increases and hence the emergence of chaotic attractors [3]. This phenomenon is often known as homoclinic explosion.

Here we report the behaviour of the strange attractors as Γ varies (with κ_0 fixed) in our numerical experiment. For each Γ we solve the pilot wave system and extract the local maxima of $a(t)$. We discard the local maxima before a certain time threshold t_{throw} to reduce the effect of transience. We then plot a bifurcation diagram for the Lorenz-like map of maxima of $a(t)$. To speed up our calculations, we start our simulation at the point where last simulation ends to reduce the transience time.

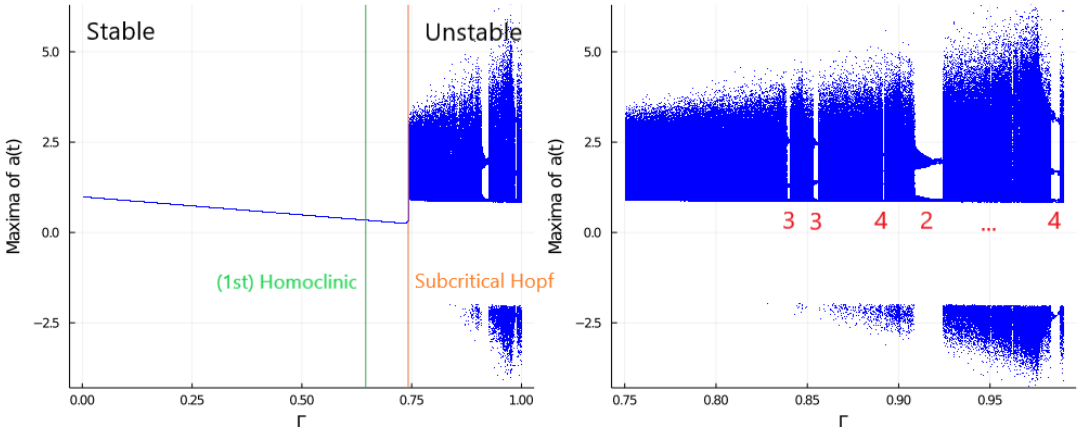

Figure 5: (a, left) The bifurcation diagram for the Lorenz like map when $\kappa_0 = 0.63$. The straight lines indicate where bifurcation happens. (b, right) An enlarged version of (a). The red numbers indicates the ”period” of the ’seemingly’ periodic windows.

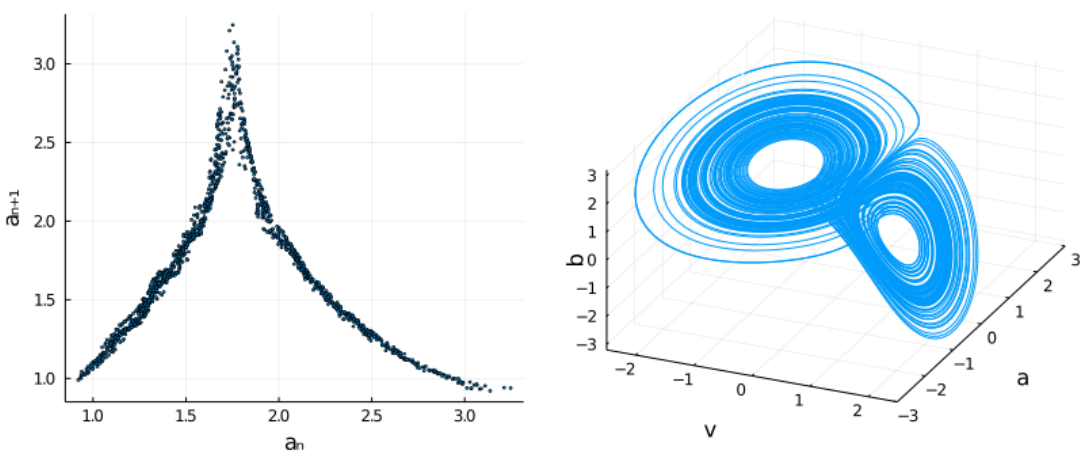

Figure 6: The (a, left) Lorenz like map and (b, right) sample trajectories when $\kappa_0 = 0.63$ and $\Gamma = 0.76$.

One would like to assert that the the pilot wave system exhibits similar chaotic features as the Lorenz system, including the generation of tent-shaped Lorenz-like map and butterfly-shaped trajectories. As we look at the bifurcation diagram for the Lorenz-like map in greater detail, we will see that the behaviour of pilot wave system is much complicated than Lorenz map. The first thing we will notice is that the ’periodic’ windows are not periodic windows. The trajectory when Γ falls into those windows may still be chaotic, even though the scale of turbulence has drastically decreased. This explains the jittering effect of propelling droplets as illustrated in [2]. It is still not clear whether there is a mathematical explanation for this.

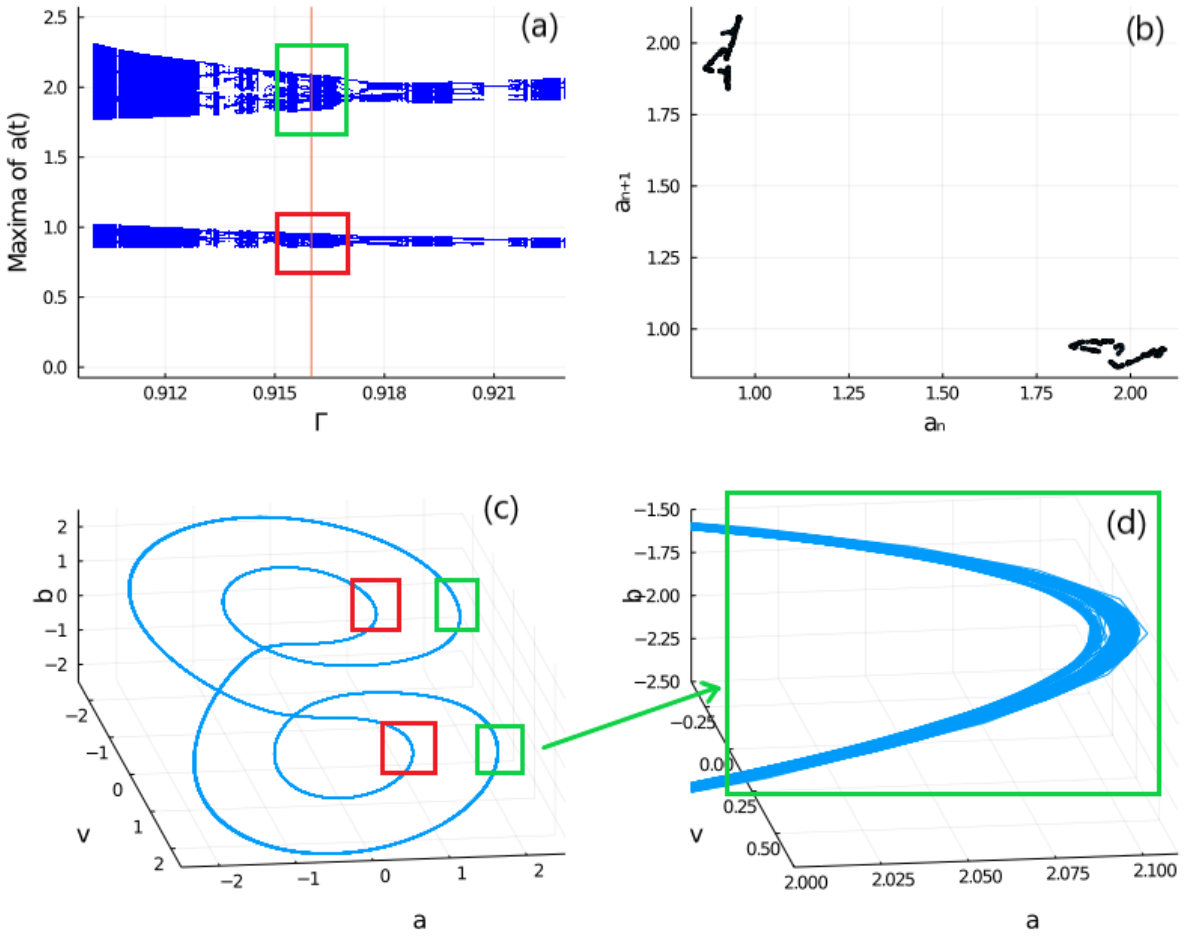

Figure 7: (a) Bifurcation diagram in Figure 5 ($\kappa_0 = 0.63$) zoomed to the 2-'periodic' window ($\Gamma \in [0.910, 9.241]$). Chaotic behaviour still exists in this window. We particularly choose $\Gamma = 0.916$ (orange line in Figure (a)) and plot the (b) Lorenz like map and (c) sample trajectory. We zoom in to obtain Figure (d) and observe a fractal-like structure of sample trajectory.

The ways that the system evolves to chaos are interesting. The pilot wave system exhibits some common features a dynamical system with quadratic non-linearity (e.g. Rossler's system) might have, for instance the period doubling cascade [4]. Nevertheless, our numerical experiments suggest that the behaviour of our system is much more complicated, which requires further investigations.

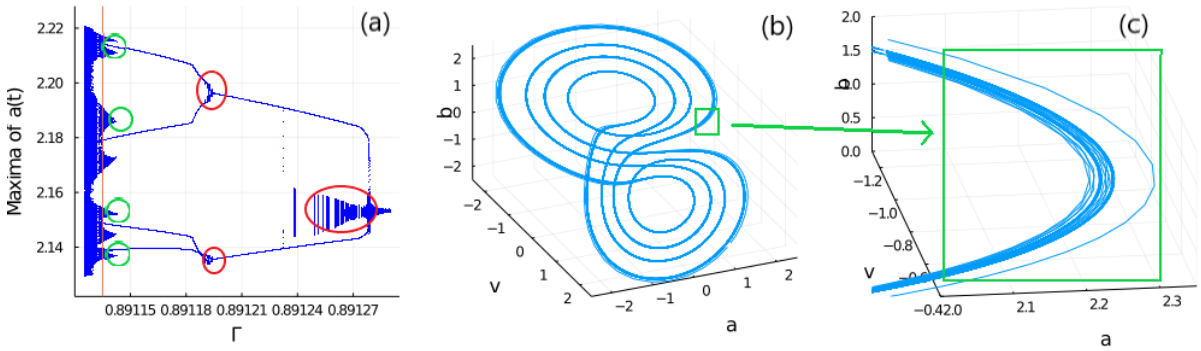

Figure 8: (a) Bifurcation diagram in Figure 5 ($\kappa_0 = 0.63$) zoomed to the window ($\Gamma \in [0.89113, 0.89129]$) where 'periodic doubling cascade' occur. Here we see the period doubling bifurcations are not sharp (circled in red). The periodic doubling cascade stopped sharply (circled in green) and the system emerges to chaos immediately. (b) Sample trajectory when $\kappa_0 = 0.63$ and $\Gamma = 0.891135$. Again the trajectory has a fractal like structure as illustrated in (c).

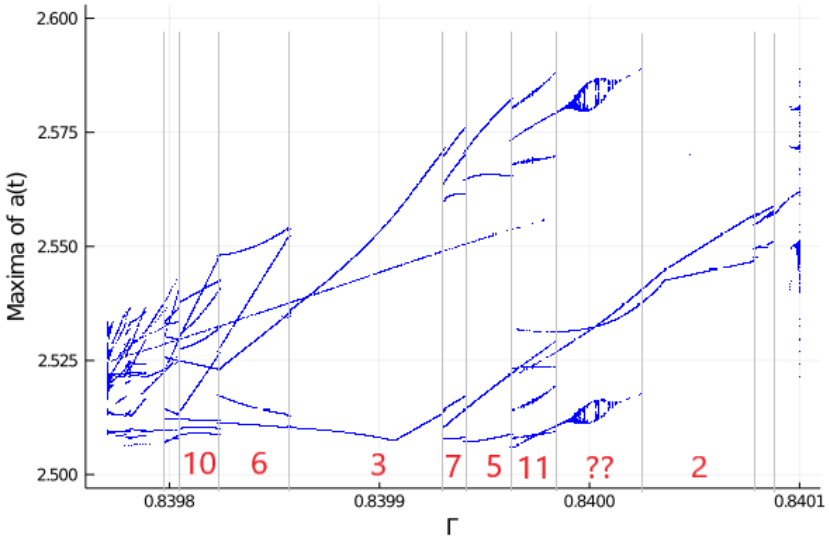

Figure 9: Bifurcation diagram in Figure 5 ($\kappa_0 = 0.63$) zoomed to the window $\Gamma \in [0.83977, 0.84010]$. The period is recorded as red numbers. Period increases (but not doubled) as Γ decreases from 0.8399 until the system becomes chaotic.

We have also varied κ_0 and look at how the bifurcation diagram evolves. We observe that for small κ_0, the bifurcation diagram exhibits a self-similar structure. As κ_0 increases, the self-similar components are squeezed away. This is consistent with the fact that chaotic behaviour is more likely to be present for small inertia (mass) [1, 2]. Here periodic doubling cascades dominate the evolution of chaos for small κ_0.

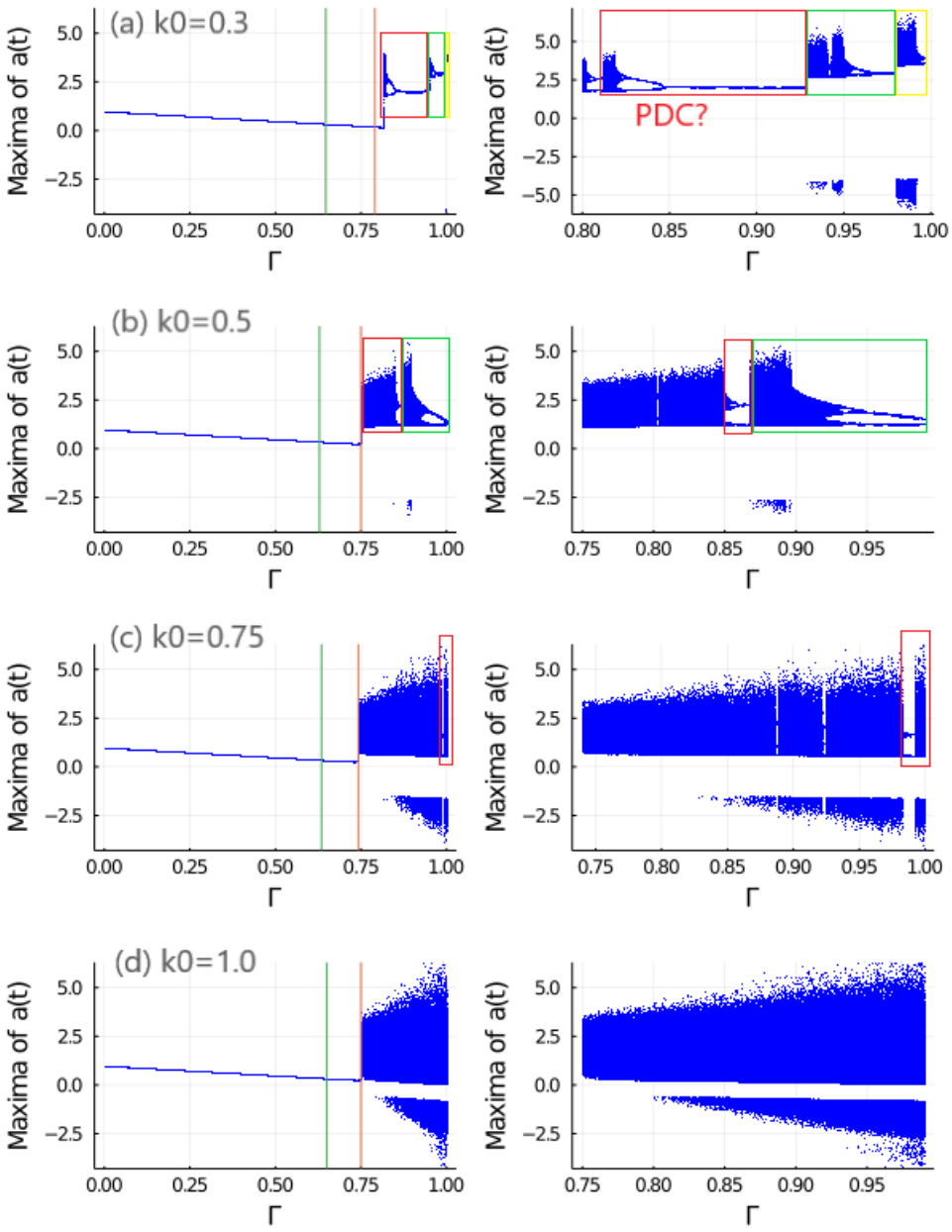

Figure 10: Bifurcation diagrams as κ_0 increases. The self-similar components have been highlighted.

4 Discussion

Section 2 indicates that the fixed points of pilot wave system has similar behaviours as Lorenz system when sufficient damping is present. Indeed, as damping μ reduces, the stable state $(0, \mu^{-1}, 0)$ destabilises via a supercritical pitchfork bifurcation, and the droplet tends to move in a constant speed. For very small damping μ, the system exhibits transient chaos and chaotic attractors. This is very similar to Lorenz system as the Rayleigh parameter r increases. However, section 3 illustrates that the ways for pilot wave system to evolve to chaos are much more complicated than Lorenz system.

Further numerical experiments and mathematical discussions are needed to study the phenomena outlined in section 3. In performing numerical experiment, one should always be careful not to run the experiment beyond time horizon [4] to ensure accuracy of numerical experiments. The rate of accumulation of numerical error is characterised by the Lyapunov constant. This could be computed by obtaining the trace of compound matrix generated by the Jacobian of the map [5, 6].

Declaration and Acknowledgements: I pledge that this essay and the work reported herein was my original work. Wherever works of others are involved, they have been cited clearly. I am grateful to Matthew Durey for extensive discussions about the design of numerical experiments. The codes for the plots are available on request.

References

[1] Anand U. Oza, Rodolfo R. Rosales, and John W. M. Bush. A trajectory equation for walking droplets: hydrodynamic pilot-wave theory. *Journal of fluid mechanics*, 737:552–570, December 2013. doi: 10.1017/jfm.2013.581. URL https://dx.doi.org/10.1017/jfm.2013.581.

[2] Matthew Durey. Bifurcations and chaos in a lorenz-like pilot-wave system. *Chaos (Woodbury, N.Y.)*, 30(10):103115, October 2020. doi: 10.1063/5.0020775. URL http://dx.doi.org/10.1063/5.0020775.

[3] Collins Sparrow. *The Lorenz Equations: Bifurcations, Chaos and Strange Attractors*, volume 41. Springer-Verlag New York Inc., New York, 1982. ISBN 9780387907758.

[4] Steven H. Strogatz. *Nonlinear Dynamics and Chaos*. Westview Press, Cambridge, Massachusetts, 1st edition, 1994. ISBN 0738204536.

[5] Jan Frøyland. Lyapunov exponents for multidimensional orbits. *Physics letters. A*, 97A(1):8–10, August 1983. doi: 10.1016/0375-9601(83)90087-7. URL http://dx.doi.org/10.1016/0375-9601(83)90087-7.

[6] Jan Frøyland and Knut H. Alfsen. Lyapunov-exponent spectra for the lorenz model. *Physical Review A*, 29:2928–2931, May 1984.